The Institute of Space and Astronautical Science
Report SP No. 17 March 2003

An Integrated Numerical Method for Predicting Aerodynamic Heating Environment for MUSES-C Entry Capsule with Ablation

By

Keisuke SAWADA*

(1 February 2003)

Abstract: An integrated numerical method to obtain trajectory-based aerodynamic heating environment for entry probe vehicles with ablation is briefly described. In this method, a thermochemical nonequilibrium CFD code is loosely coupled with an ablation module along the entry trajectory. Radiative heating is estimated by the use of multi-band radiation module. The effect of earlier turbulent transition of the boundary layer due to ablation product gas is included. Calculated results for MUSES-C sample return capsule are shown and that are compared with the results of existing analysis.

1. INTRODUCTION

Ablation of heatshield during entry flight is essentially a time dependent phenomenon because the amount of ablation is affected by the net heating rate that varies along the entry trajectory. Furthermore, the net heating rate itself is critically affected by ablation because ablation reduces the convective heating rate by so-called convective blockage effect. Therefore, the accurate prediction of heating environment with ablation is only available when a coupled analysis of flowfield and thermal response of ablator is accomplished along the entry trajectory.

The situation can be further complicated if we consider strongly radiating flowfield such as that occurred in the entry flight of Galileo probe vehicle. Emission and absorption of radiation change temperature of the flowfield that alters the property of radiation, and thus constitutes a coupling problem. Shape change of heatshield due to surface recession can have influence over heating rate. This in turn changes the recession rate. These are typical examples that show how various issues are closely related to each other, and why a trajectory-based aerodynamic heating problem should be solved iteratively by an integrated numerical method.

The flow features that should be considered in the integrated numerical method are (i) thermochemical nonequilibrium of high temperature flowfield with ablation products, (ii) thermal response of ablative heatshield, (iii) radiative heat transfer coupled with the flowfield, (iv) shape

* Department of Aeronautics and Space Engineering, Tohoku University, Sendai 980–8579, JAPAN.

change of heatshield due to surface recession, (v) effect of spalled particles, and (vi) injection induced turbulence due to ablation product gas (Suzuki T. et al. 2002). For example, the analysis of Galileo entry flowfield requires all of these flow features to be fully considered. In case of the Pioneer-Venus probe vehicles, those (iv) and (v) and coupling effect of the flowfield and radiation in (iii) may be neglected. However, our previous study has indicated that (vi) should be taken into account for accurate reproduction of flight data (Takahashi & Sawada 2002). The required flow features for an analysis of MUSES-C reentry flight may be the same as those for Pioneer-Venus case, because the entry velocity and entry angle are similar.

Validation of analysis code is very important for future design of ablative heatshield. In order to accomplish this, the flight data obtained in the past entry flight, such as Apollo entry capsule, Pioneer-Venus entry probes, and Galileo probe provide unique opportunities for validation (Park 1999). Some of the results in our previous studies for developing an integrated analysis method for entry flight heating environment and its validation can be found in references (Izawa & Sawada 2000a; Suzuki T. et al. 2002; Takahashi & Sawada 2002). In this work, we first give a brief description of numerical methods that constitute the integrated analysis code. We then show the calculated results for MUSES-C entry flight, and give the related discussions.

2. NUMERICAL METHODS

2.1 Outline of CFD Module

In the computational fluid dynamics (CFD) module, we solve the Navier-Stokes equations that account for thermochemical nonequilibrium reactions. Because we must deal with two different gas flows, i.e., the freestream gas and the ablation product gas, that have different chemical compositions, we cannot assume a constant elemental ratio of freestream gas (Park 1989) to the entire computational domain. Therefore, we instead employ the concept of elemental density conservation equations proposed by Hassan et al. (1992).

In the analysis of MUSES-C entry flight, we assume 11 chemical species for high temperature air (N, O, N_2, O_2, NO, N^+, O^+, N_2^+, O_2^+, NO^+, e^-), and 10 chemical species for ablation product gas (C, C_2, C_3, CO, CN, C^+, H, H_2, C_2H, H^+). Therefore, we have 21 species conservation equations in total. Instead of solving all of these species conservation equations, we introduce conservation equations for those elemental densities of $\tilde{\rho}_N$, $\tilde{\rho}_O$, $\tilde{\rho}_C$, $\tilde{\rho}_H$, and properly remove the same number of species conservation equations. These elemental densities are related to the densities of chemical species by the following equations:

$$\frac{\tilde{\rho}_N}{M_N} = \frac{\rho_N}{M_N} + 2\frac{\rho_{N_2}}{M_{N_2}} + \frac{\rho_{NO}}{M_{NO}} + \frac{\rho_{N^+}}{M_{N^+}} + \frac{\rho_{N_2^+}}{M_{N_2^+}} + \frac{\rho_{NO^+}}{M_{NO^+}} + \frac{\rho_{CN}}{M_{CN}}, \tag{1a}$$

$$\frac{\tilde{\rho}_O}{M_O} = \frac{\rho_O}{M_O} + 2\frac{\rho_{O_2}}{M_{O_2}} + \frac{\rho_{NO}}{M_{NO}} + \frac{\rho_{O^+}}{M_{O^+}} + \frac{\rho_{O_2^+}}{M_{O_2^+}} + \frac{\rho_{NO^+}}{M_{NO^+}} + \frac{\rho_{CO}}{M_{CO}}, \tag{1b}$$

$$\frac{\tilde{\rho}_C}{M_C} = \frac{\rho_C}{M_C} + 2\frac{\rho_{C_2}}{M_{C_2}} + \frac{\rho_{CN}}{M_{CN}} + \frac{\rho_{CO}}{M_{CO}} + \frac{\rho_{C_3}}{M_{C_3}} + \frac{\rho_{C^+}}{M_{C^+}} + \frac{\rho_{C_2H}}{M_{C_2H}}, \tag{1c}$$

$$\frac{\tilde{\rho}_H}{M_H} = \frac{\rho_H}{M_H} + 2\frac{\rho_{H_2}}{M_{H_2}} + \frac{\rho_{C_2H}}{M_{C_2H}} + \frac{\rho_{H^+}}{M_{H^+}}. \tag{1d}$$

Note that these are simple statements that number density of each element is the same. The total density ρ is given by a sum of these elemental densities as

$$\rho = \tilde{\rho}_N + \tilde{\rho}_O + \tilde{\rho}_C + \tilde{\rho}_H. \tag{2}$$

One can show that the governing equations for these elemental densities can be written as

$$\frac{\partial \tilde{\rho}_s}{\partial t} + \frac{\partial}{\partial x_j}\left(\tilde{\rho}_s u_j\right) = \frac{\partial}{\partial x_j}\left(\rho D \frac{\partial \tilde{c}_s}{\partial x_j}\right), \tag{3}$$

where s denotes the elemental species, u_j the mass averaged velocity component, D the diffusion coefficient, and $\tilde{c}_s$ the mass fraction of elemental species s.

We now have 21 species conservation equations, 4 elemental density conservation equations, and a total density conservation equation. We remove 4 species density conservation equations for N_2, O_2, C_2, H_2, and retain 4 conservation equations for elemental densities. These densities of removed chemical species conservation equations can be found by solving Eq. (1). Moreover, we remove the total density conservation equation because we have Eq. (2). Therefore, we solve 17 species conservation equations and 4 elemental density conservation equations for 21 chemical species. We also solve two momentum equations, a total energy equation, and a vibrational-electronic energy conservation equation. All of these conservation equations are independent to each other.

Park's two-temperature model (Park 1989) is employed to describe the nonequilibrium thermochemical states. The molecular viscosity for each chemical species is either given by Blottner's model (Blottner et al. 1971) or by a curve-fit. The thermal conductivity is given by Eucken's relation (Vincenti & Kruger 1967). The total viscosity and conductivity are calculated using Wilke's empirical mixing formula (Wilke 1950). We assume the diffusion coefficient to be constant for all species with a constant Schmit number of 0.5.

The governing equations are integrated by the cell-centered finite volume scheme utilizing AUSM-DV numerical flux (Wada & Liou 1994) and MUSCL approach for attaining higher order spatial accuracy. In the time integration, the LU-SGS algorithm is employed for obtaining a faster convergence, which is combined with the diagonal point implicit method (Eberhardt & Imlay 1992) for stability maintenance of reaction terms.

2.2 Outline of Material Thermal Response Code

Ahn et al. (2002) developed a computer code named Super Charring Materials Ablation (SCMA) in order to study the thermal response of ablator for Pioneer-Venus entry capsules. In the SCMA code, four conservation equations, i.e., conservation of solid density, pyrolysis gas density, momentum of pyrolysis gas, and total energy are solved one-dimensionally.

A unique feature of the present SCMA code is that it solves the momentum equation of pyrolysis gas. Therefore, one can include various phenomena related to gas motions, such as friction and inertial forces. This is in contrast with the existing CMA code or HBI method where steady flow assumption was made to eliminate this equation. Details of the code and results of the code validation study can be available in the reference.

2.3 Surface Reactions

In the MUSES-C entry flight calculation, we consider the following four types of chemical reactions that occur at the ablator surface: (i) surface oxidation that produces CO, (ii) surface nitridation that produces CN, (iii) surface sublimation that produces C_3, and (iv) recombination of ions and electrons. The concentration of surface reacting species can be found by solving the relation that the production rate at the wall balances with diffusion (Suzuki T. et al. 2002).

2.4 Radiation Module

The radiative heat flux at the wall surface is computed from the obtained flowfield by solving the radiative transfer equation with the tangent-slab approximation. The emission and absorption coefficients are first calculated using a multiband model that considers $O(10^3)$ wavelength points. For example, in the analysis of MUSES-C entry capsule, 2294 wavelength points are chosen for air and 7610 wavelength points for ablation product gas in the wavelength range from 750 to 15000Å. The absorption coefficient of the gas mixture is expressed as a sum of those for individual species in the form of (Park & Milos 1990)

$$\kappa_\lambda = \sum_s n_s \sigma_{\lambda_s}, \tag{4}$$

in which n_s denotes the number density and σ_{λ_s} the absorption cross section at given wavelength value for chemical species s. The cross section value is curve fitted using five parameters in the form of

$$\sigma_{\lambda_s} = \exp\left(A^s_{\lambda_1}/z + A^s_{\lambda_2} + A^s_{\lambda_3} \ln z + A^s_{\lambda_4} z + A^s_{\lambda_5} z^2\right), \tag{5}$$

where $z = 10000/T_v$ with T_v denoting the vibrational temperature.

2.5 Turbulence Model

Ablation product gas that is injected into the boundary layer from the wall surface is assumed as inherently turbulent according to the concept of injection-induced turbulence that was proposed by Park (1984). The employed turbulence model can be written as a sum of eddy viscosity given by the Park's model and also the turbulence model of Baldwin & Lomax (1978) as

$$\mu_t = (\mu_t)_{inj} + (\mu_t)_{BL}. \tag{6}$$

The first term is given by

$$(\mu_t)_{inj} = \rho d^2 |\omega|, \tag{7}$$

where ω denotes vorticity. The mixing length d is defined by

$$d = \max(0, d_w - 0.4y) \exp\left(-y^+/A^+\right), \tag{8}$$

in which d_w gives the wall mixing length that takes the maximum value at the wall, and decays exponentially in the boundary layer according to Van Driest theory (Van Driest 1956). The subscript w indicates the wall value. The wall mixing length d_w is given by the relation

$$(\mu_t)_{Park} = \rho_w d_w^2 |\omega|_w \tag{9}$$

2.6 Coupling Method

First, let us describe how the wall boundary conditions are given in the present calculations. Note that the wall properties are iteratively determined through coupling between CFD and SCMA modules. The mass injection rate of pyrolysis gas from the wall is given by the SCMA code as

$$\dot{m}_p = \varepsilon \rho_p u_p, \tag{10}$$

where subscript p denotes pyrolysis gas. The void fraction ε represents the degree of porosity for ablator. Because the SCMA code gives the void fraction one-dimensionally to the wall surface, we assume the porosity at the wall is identical with the void fraction. Therefore, at the wall, the ratio of void portion and catalytic wall mostly consisting of char is given by $\varepsilon : 1 - \varepsilon$.

The chemical composition of ablation product gas at the wall surface is calculated by assuming thermochemical equilibrium condition. The surface pressure is given by CFD solution while the surface temperature by the SCMA code. The SCMA code requires surface heat flux along the entry trajectory as the boundary condition. Such heat flux is provided by CFD solution at the chosen trajectory points. At intermediate time between two trajectory points, heat flux value is interpolated either by a linear or a quadratic function. Note that the heat flux value at the new trajectory point depends not only on the heat flux value at the previous trajectory point, but also on the intermediate heat flux value that is interpolated using the heat flux at the new trajectory point. Therefore, the heat flux value at the new trajectory point needs to be given by CFD solution iteratively.

The coupling of radiative heat transfer in this calculation is indirectly made. Once the radiative heat flux is obtained from CFD solution, it is fed into the SCMA code as a part of the net heating rate at the wall surface. The SCMA code returns the surface temperature and mass injection rate that influence the entire flowfield and radiation. Therefore, the flowfield and radiation is coupled through the boundary condition. A direct coupling between the flowfield and radiation needs to be considered in the case of Galileo, but can be neglected in the case of MUSES-C.

As to the surface recession, the SCMA code itself does not take account of surface recession explicitly. It is implicitly accounted in the code by changing the position of the outer wall surface and redraws the numerical mesh inside of the ablator. In the CFD calculation, one can include the effect of surface recession by changing the shape of capsule at each trajectory point. However, such effect has not been considered in this study simply because the amount of surface recession is negligibly small.

2.7 Code Validation History

The results of validation studies for each component of computer codes that constitute the present integrated analysis method are summarized here. The thermochemical package used in the CFD code was originally developed for airflows accounting for five neutral air species. Using this package, Niizuma & Sawada (1997) attempted to reproduce Fay-Riddell correlation of the blunt body convective heating rate, and obtained a good agreement with theoretical values. They also obtained a fair agreement of heat flux at the nose of space shuttle with the corresponding flight data. The package has also been checked extensively in a series of calculation of shock layer thickness over a sphere and a cone in intermediate hypersonic range (Furudate et al. 1999a, 1999b). The package was also extended to include carbonaceous species and was applied to solve the entry flowfield of Pioneer-Venus probes (Izawa & Sawada 2000a; Takahashi & Sawada 2002).

The SCMA code developed by Ahn et al. (2002) was validated by the comparison with the experimental data obtained in arc heated airflow and was applied to solve the thermal response of abltive heatshield for Pioneer-Venus probe vehicles. The SCMA code was also examined in detail of the ablator material of MUSES-C (Ahn 1998).

The injection-induced turbulence model was first incorporated into a CFD code by combining with one-equation turbulence model. The code was applied to obtain the velocity profile

in the boundary layer over a spherical blunt body with foreign gas injection through a porous wall. A peculiar velocity profile seen in the experimental data was qualitatively reproduced (Dendou & Sawada 1998). Izawa & Sawada (2000b) studied an alternative method for combining the injection-induced turbulence model with a CFD code by employing a zero equation turbulence model. This new scheme successfully reproduced the surface heat transfer rate at the stagnation point of a blunt body with a foreign gas injection in the hypersonic flowfield. Though the heating rate at the downstream side was overestimated by a factor of 2, the overall agreement with the experiment was judged fair. With the use of this new scheme, the entry flowfield of Pioneer-Venus probe vehicles with ablation was calculated. A reasonable agreement with the flight data was obtained for the temperature history not only at the stagnation point but also at the frustum region (Izawa & Sawada 2000a; Takahashi & Sawada 2002).

3. MUSES-C ENTRY FLIGHT SIMULATION

Figure 1 shows the chosen trajectory points for CFD calculations along the entry trajectory of MUSES-C. The entry angle is assumed as -12 deg at an altitude of 200 km. Figure 2 shows a typical example of computational mesh system with 59×77 grid points. It covers the forebody part of MUSES-C capsule.

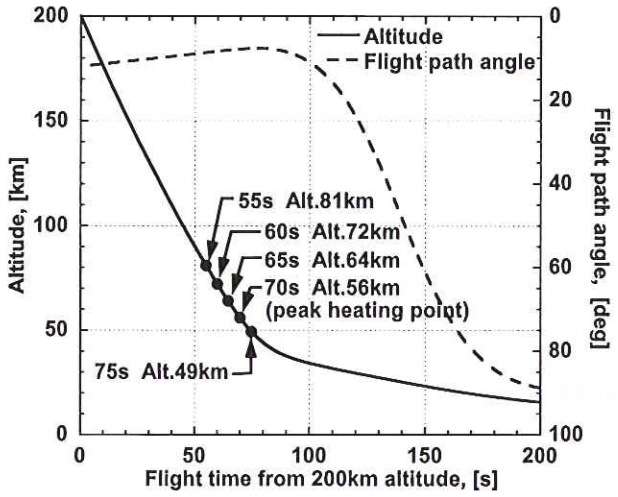

Fig. 1: Entry trajectory of MUSES-C. Entry angle is -12 deg at 200 km. Trajectory points for CFD calculations are indicated.

Calculation starts from obtaining an initial CFD solution at the first trajectory point at 55 sec of flight time. We assume that ablation is absent and that the boundary layer is laminar. A constant wall temperature of 3000 K is arbitrarily chosen. From this initial solution, we then obtain thermal response of ablator from the beginning of entry flight to this first trajectory point. We assume the wall heat flux is zero before 30 sec of flight time (density is below 1.0×10^{-7} kg/m^3) and interpolate it by a quadratic function up to the first trajectory point. Putting the obtained heat flux profile along the entry trajectory into the SCMA code, we can find the temperature and injection rate at the wall surface at the first trajectory point. These values are used as the new boundary conditions for CFD calculation. We then obtain the new CFD solution that accounts for ablation and turbulence effect at the same trajectory point.

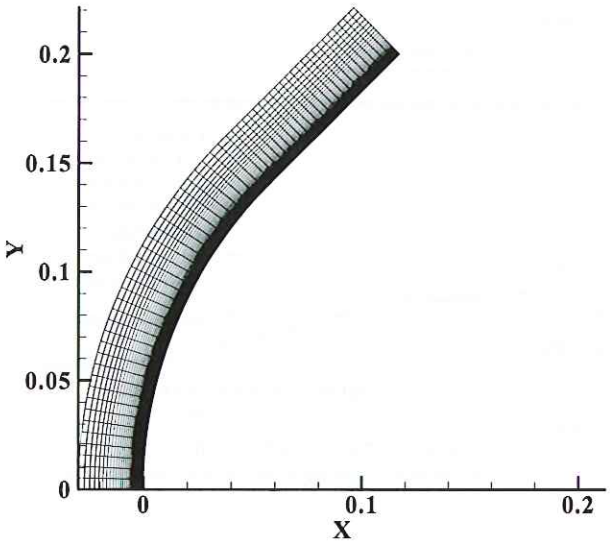

Fig. 2: Example of computational mesh with 59×77 grid points.

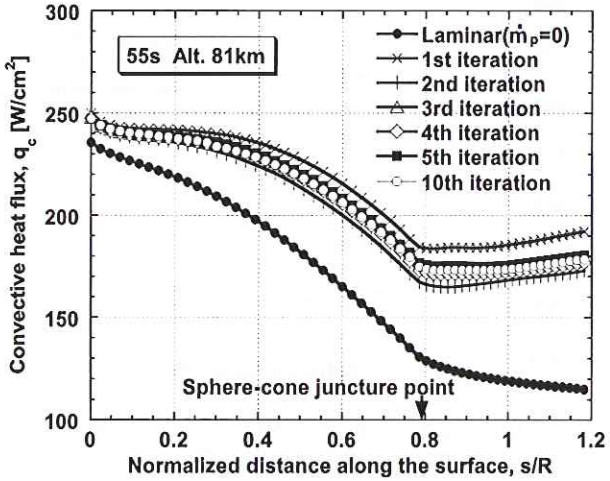

Fig. 3: Convergence history of convective heat flux profile along the surface with ablation at 55 sec from 200 km.

The new CFD solution in turn gives the new wall heat flux value. We specify the new heat flux profile along the trajectory and put it again into the SCMA code. These iterative procedures are continued until the wall heat flux profile is converged.

Figure 3 shows the convergence history of convective heat flux along the body surface at 55 sec from 200 km. One can see that the convergence is virtually attained within 5 iterations. The wall heat flux given by the turbulent solution becomes larger than that given by the initial laminar solution without ablation even at the stagnation point. The convective blockage effect of ablation product gas is totally cancelled by the effect of assumed turbulence. The convergence history of wall temperature for this altitude is plotted in Fig. 4. The wall temperature substantially decreases from the initially assumed wall temperature due to ablation.

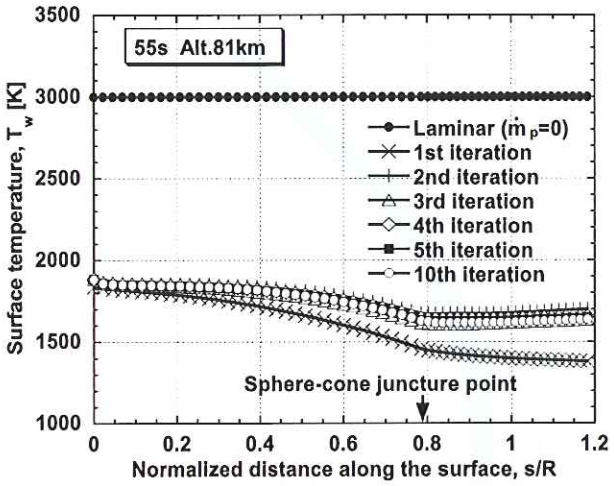

Fig. 4: Convergence history of wall temperature profile along the surface with ablation at 55 sec from 200 km.

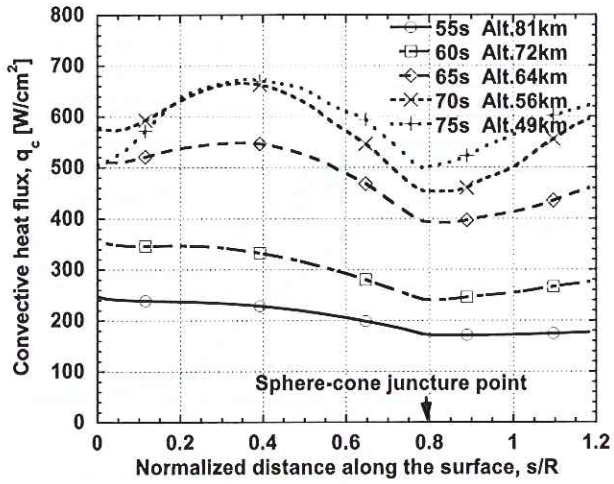

Fig. 5: Converged profile of the convective heat flux along the surface at the chosen trajectory point.

Next, we try to obtain the CFD solution at 60 sec of flight time. As before, we assume the initial flowfield to be laminar and without ablation. We then linearly interpolate the heat flux value from 55 sec to 60 sec, which is fed into the SCMA code. The solution from the SCMA code gives the wall temperature and injection rate at 60 sec that are put into the CFD code as the boundary conditions. The converged and consistent solution accounting for ablation at 60 sec is finally obtained iteratively. The converged solutions at later flight time are similarly obtained. The surface heating profile accounting for ablation and turbulence at the chosen trajectory points are summarized in Fig. 5. Because of the turbulent heating, the heating rate in the downstream region becomes larger particularly at 70 and 75 sec of flight time.

Figure 6 shows the stagnation point heat transfer rates with ablation along the entry trajectory. The total heat flux is defined as a sum of the convective heat flux and the wallward

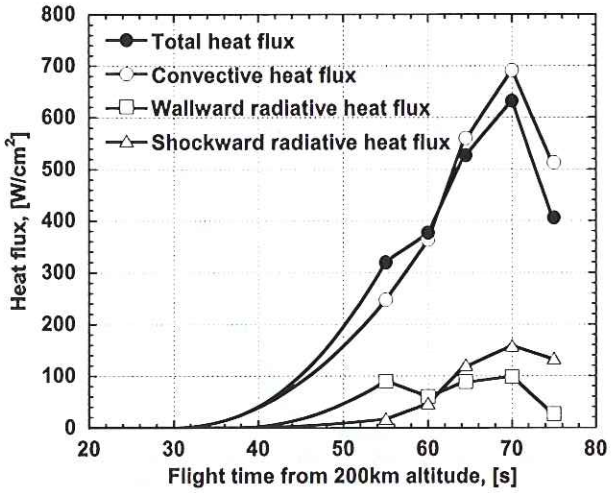

Fig. 6: Heat flux along the entry trajectory at the stagnation point.

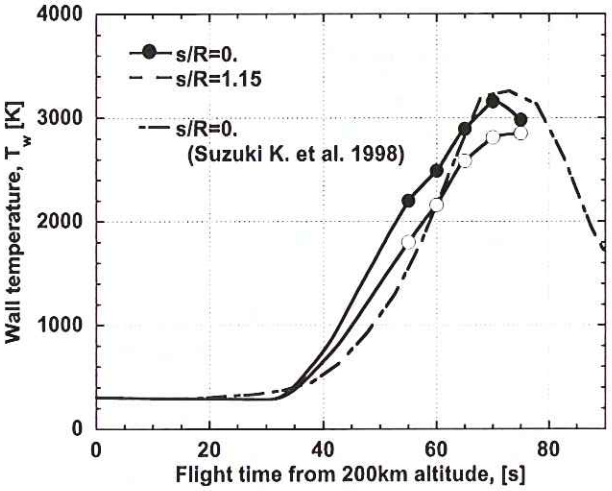

Fig. 7: Wall temperature histories at the stagnation point and in the downstream region of MUSES-C reentry capsule.

radiative heat flux minus the shockward radiative heat flux from the wall. A maximum convective heat flux value of about 700 W/cm^2 is obtained at 70 sec. The wallward radiative heat flux is about 15 % of the convective heat flux at this peak heating point.

The obtained temperature histories at the ablator surface are shown in Fig. 7. At the stagnation point, the present temperature history agrees fairly well with that given by Suzuki K. et al. (1998). They studied the stagnation heating and ablation process of the MUSES-C capsule by using the laminar viscous shock layer equations. A fair agreement of heat flux value is attained because Suzuki K. et al. (1998) considered the catalytic recombination of O and N atoms at the wall surface but not the effect of turbulence, while the present study consider the effect of turbulence that significantly enhances the heating rate but not the catalytic recombination. One can see that the temperature at the frustum edge is elevated and becomes

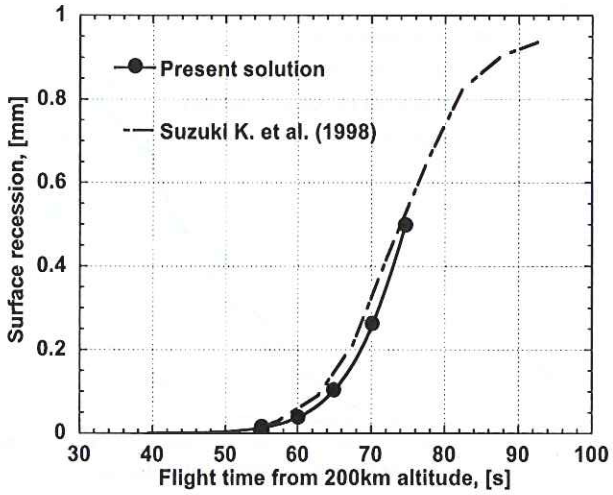

Fig. 8: Computed surface recession at the stagnation point along the entry trajectory.

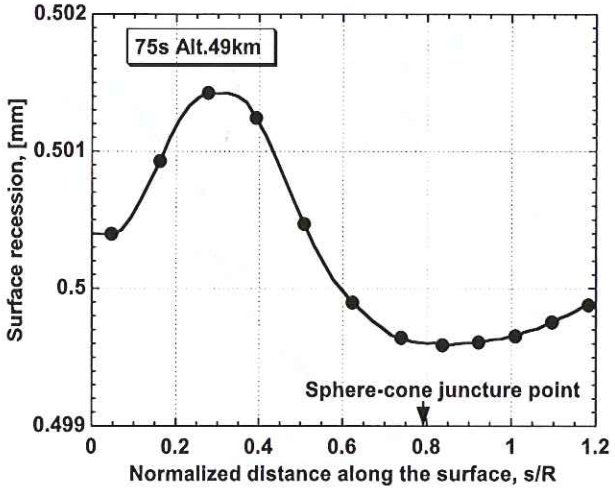

Fig. 9: Computed surface recession along the surface at 75 sec from 200 km.

comparable with that at the stagnation point due to turbulence effect.

The computed surface recession at the stagnation point is shown in Fig. 8. Although the present solution is slightly shifted from that given by Suzuki K. et al. (1998), the agreement between these solutions is fairly good. The calculated recession profile along the wall surface at the last trajectory point is shown in Fig. 9. Because of the significant turbulent heating, the surface recession becomes larger at $s/R = 0.3$ than that at the stagnation point, and it then gradually decreases toward the juncture point but slightly increases again at the frustum edge.

4. DISCUSSIONS

In this work, we first describe a trajectory-based integrated analysis code briefly. This integrated analysis code consists mainly of CFD module, SCMA module, and radiation module.

The coupling method of these modules is also explained. A short validation history of these modules and the integrated code is given. The calculated results of heating environment for MUSES-C sample return capsule by this integrated analysis code are shown. It is shown that the converged solution along the entry trajectory can be obtained by loosely coupling approach between the CFD and SCMA codes. The convergence at each trajectory point is reached within a few iterations.

The maximum convective heat flux at the stagnation point is found to be about 700 W/cm^2 at the peak heating point, whereas the wallward radiative heat flux becomes only about 15 % of the convective heat flux value. The wall temperature as well as the surface recession rate at the stagnation point along the entry trajectory duplicates well with that given by the existing analysis. This agreement is attained because the catalytic recombination of atoms at the wall surface is included in the existing analysis, whereas the present calculation assumes a noncatalytic wall for those recombination reactions but includes the turbulence effect of the ablation product gas.

It is found that the wall temperature at the downstream frustum region is significantly elevated by the effect of turbulence. This phenomenon was also observed in the numerical analysis of aerodynamic heating environment for the Pioneer-Venus entry probes. The actual flight data also indicated such phenomenon was really the case. Therefore it will be interesting to see whether the actual flight data of MUSES-C will confirm the present prediction of higher heating rate that will occur in the downstream frustum region.

It is indeed important to assess the integrated analysis code in terms of how well the available flight data into a planetary atmosphere can be reproduced. Our continuous efforts have been focused on this issue. So far, we have succeeded in obtaining a reasonable agreement of temperature profiles with those taken in the entry flights of the Pioneer-Venus probe vehicles (Takahashi & Sawada 2002). Our next target is to reproduce the peculiar recession profile of Galileo probe ablator that was reconstructed from the actual flight data (Milos 1996). For this purpose, we are now trying to develop a numerical method for computing strongly radiating flowfield for Jovian entry flight. Preliminary results are already shown in the work of Matsuyama et al. (2002).

ACKNOWLEDGMENT

The author would like to thank Suzuki, T., a graduate student in the Department of Aeronautics and Space Engineering, Tohoku University, who have contributed in developing the present integrated analysis code, and also obtaining calculated results for MUSES-C entry flight that are shown in the present article.

REFERENCES

Ahn H.-K., 1998, Heatshield Problems of Pioneer-Venus and MUSES-C, Ph.D. Dissertation, Dept. of Aeronautics and Space Engineering, Tohoku University, Sendai, Japan.

Ahn H.-K., Park C., Sawada K., 2002, Response of Heatshield Material at Stagnation Point of Pioneer-Venus Probe, Journal of Thermophysics and Heat Transfer, Vol. 16, No. 3, pp. 432–439.

Baldwin B. S., Lomax H., 1978, Thin Layer Approximation and Algebraic Model for Separated Turbulent Flows, AIAA Paper 78-257

Blottner F. G., Johnson M., Ellis, M., 1971, Chemically Reacting Viscous Flow Program for Multi-Component Gas Mixture, Sandia National Lab., Rept. SC-RR-70-754

Dendou E., Sawada K., 1998, Numerical Simulation of Hypersonic Flow over a Sphere with Surface Injection, AIAA Paper 98–0773.

Eberhardt S., Imlay S., 1992, Diagonal Implicit Scheme for Computing Flows with Finite Rate Chemistry, Journal of Thermophysics and Heat Transfer, Vol. 6, No. 2, pp. 208–216.

Furudate M., Nonaka S., Sawada K., 1999, Behavior of Two-Temperature Model in Intermediate Hypersonic Regime, Journal of Thermophysics and Heat Transfer, Vol. 13, No. 4, pp. 424–430.

Furudate M., Nonaka S., Sawada K., 1999, Calculation of Shock Shapes over Simple Geometry in Intermediate Hypersonic Air Flow, AIAA Paper 99-3686.

Hassan B., Candler G. V., Olynick D. R., 1992, The Effect of Thermochemical Nonequilibrium on the Aerobraking Vehicles, AIAA Paper 92–2877.

Izawa Y., Sawada K., 2000a, Calculation of Hypersonic Flow with Ablation for Pioneer-Venus Probe, AIAA Paper 2000–0208.

Izawa Y., Sawada K., 2000, Calculation of Surface Heat Transfer for a Sphere with Wall Injection, Journal of Thermophysics and Heat Transfer, Vol. 14, No. 2, pp. 230–236.

Matsuyama S., Shimogonya Y., Ohnishi N., Sawada K, Sasoh, A., 2002, Numerical Simulation of Galileo Probe Entry Flowfield with Radiation, AIAA Paper 2002–2994.

Milos F. S., 1996, Galileo Probe Heat Shield Ablation Experiment, AIAA Paper 96–1823.

Niizuma K., Sawada K., 1997, Nonequilibrium Flow Computation for the Space Shuttle Nose Using Unstructured Meshes, AIAA Paper 97–2548.

Park C., 1984, Injection-Induced Turbulence in Stagnation-Point Boundary Layers, AIAA Journal, Vol. 22, No. 2, pp. 219–225.

Park C., 1989, Nonequilibrium Hypersonic Aerothermodynamics, John Wiley and Sons Inc., New York

Park C., Milos F. S., 1990, Computational Equations for Radiating and Ablating Shock Layers, AIAA Paper 90–0356.

Park C., 1999, Heatshielding Problems of Planetary Entry, A Review, AIAA Paper 99–3415.

Suzuki K., Fujita K., Abe T., 1998, Trajectory-based Coupled Analysis of Viscous Shock-Layer and Charring Ablator for Stagnation Heating Environment of MUSES-C Re-Entry Capsule, Symposium on Flight Mechanics and Astrodynamics, The Institute of Space and Astronautical Science, pp. 117–120. (in Japanese)

Suzuki T., Furudate M., Sawada K., 2002, Unified Calculation of Hypersonic Flowfield for a Reentry Vehicle, Journal of Thermophysics and Heat Transfer Vol. 16, No. 1, pp. 94–100.

Takahashi M., Sawada, K., 2002, Simulation of Entry Flight Flowfield over Four Probe Vehicles in Pioneer-Venus Mission, AIAA Paper 2002–0909.

Van Driest E. R., 1956, On Turbulent Flow Near a Wall, Journal of Aerospace Science, Vol. 23, No. 11, pp. 1007–1011.

Vincenti W. G., Kruger C. H., 1967, Introduction to Physical Gas Dynamics, Wiley, New York, pp. 375–435.

Wada Y., Liou M. S., 1994, A Flux Splitting Scheme with High Resolution and Robustness for Discontinuities, AIAA Paper 94–0083.

Wilke C. R., 1950, A Viscosity Equation for Gas Mixtures, Journal of Chemical Physics, Vol. 18, No. 4, pp. 517–519.